Design Rules for Sequestration of Viruses into Polypeptide Complex Coacervates

Supplementary Information

Design Rules for Sequestration of Viruses Into Polypeptide-based Complex Coacervates

Pratik U. Joshi[1,2], Claire Decker[1], Xianci Zeng[3], Arvind Sathyavageeswaran[3,],

Sarah L. Perry[3,4]*, Caryn L. Heldt[1,2,]*

[1]Department of Chemical Engineering, Michigan Technological University, Houghton, MI 49931, USA

[2]Health Research Institute, Michigan Technological University, Houghton, MI 49931, USA

[3]Department of Chemical Engineering, University of Massachusetts Amherst, Amherst, MA 01003, USA

[4]Institute for Applied Life Sciences, University of Massachusetts Amherst, Amherst, MA 01003, USA

*Correspondence: heldt@mtu.edu, perrys@engin.umass.edu

Summary of Contents:

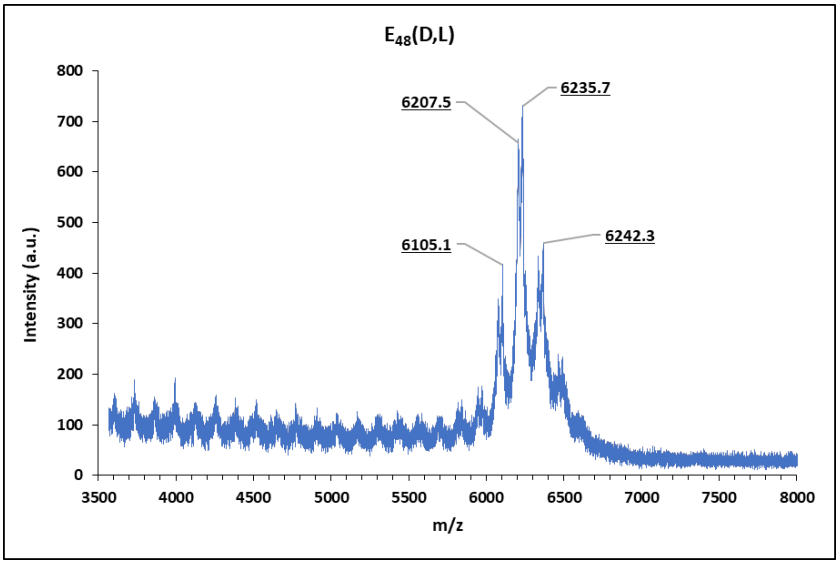

Figure S1a. MALDI spectrum of E_{48}. The expected theoretical mass is 6214.5 g/mol, excluding counterions. The maximum observed at m/z = 6235.7 could correspond to the presence of a Na^+ counterion. The peak at m/z = 6105.1 suggests a possible missing glutamate residue.

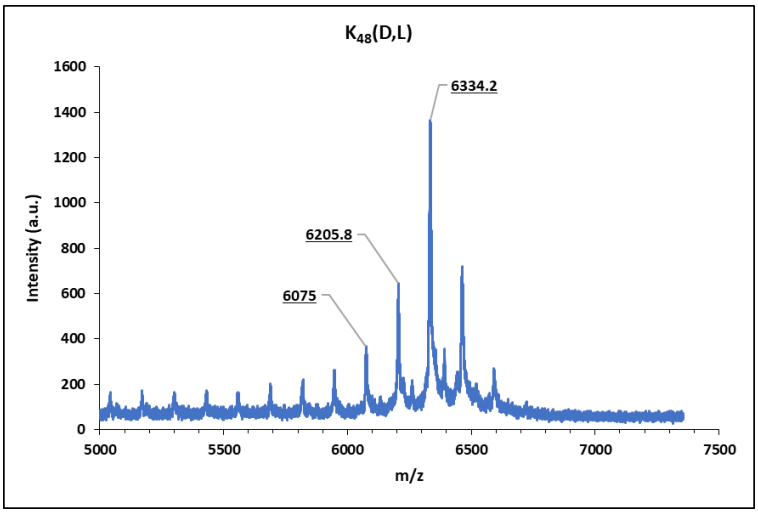

Figure S1b. MALDI spectrum of K_{48}. The expected theoretical mass is 6169.3 g/mol, excluding counterions. The maximum observed at m/z = 6334.2 could correspond to the presence of a combination of TFA^- and two Na^+ counterions. The peaks at m/z = 6205.8 and 6075.0 suggest possible missing lysine residues, as do the subsequent smaller but equally spaced peaks.

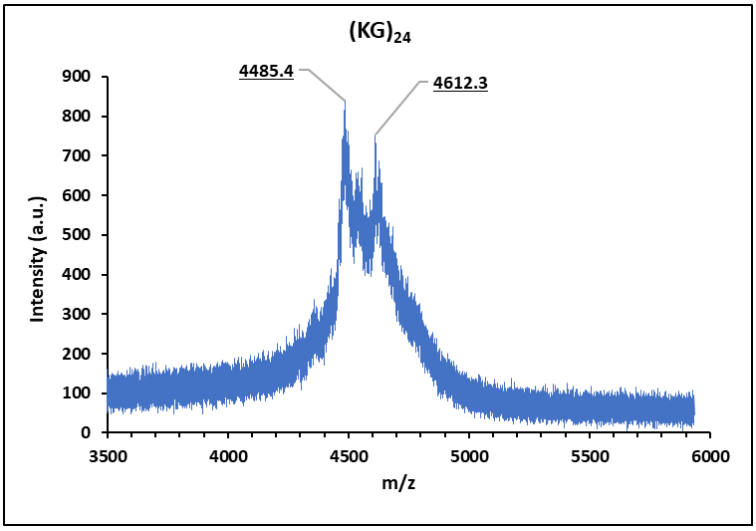

Figure S1c. MALDI spectrum of $(KG)_{24}$. The expected theoretical mass is 4462.4 g/mol, excluding counterions. The maximum observed at m/z = 4485.4 could correspond to the presence of a Na^+ counterion.

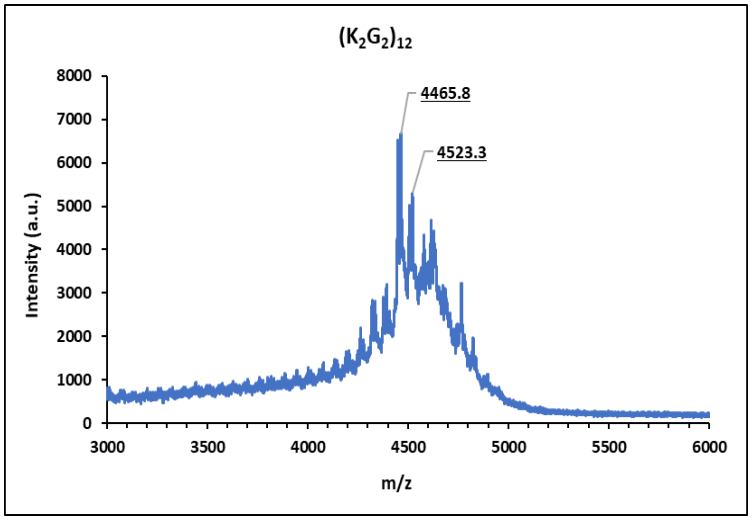

Figure S1d. MALDI spectrum of $(K_2G_2)_{12}$. The expected theoretical mass is 4462.4 g/mol, excluding counterions. The maximum observed at m/z = 4465.8 could correspond to the protonated form of the peptide.

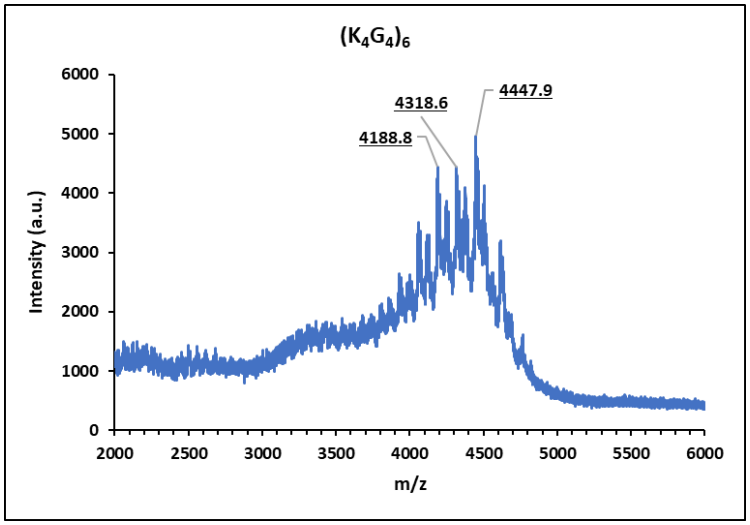

Figure S1e. MALDI spectrum of $(K_4G_4)_6$. The expected theoretical mass is 4462.4 g/mol, excluding counterions. The maximum was observed at m/z = 4447.9. The peak at 4318.6 could correspond to a missing lysine residue.

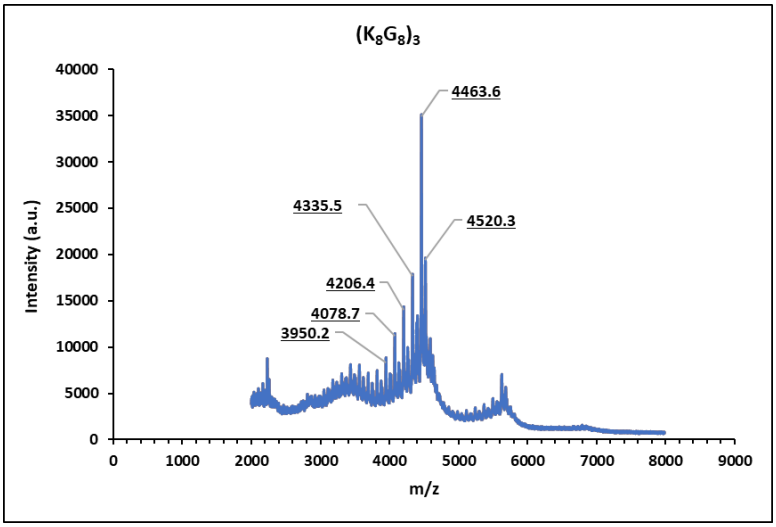

Figure S1f. MALDI spectrum of $(K_8G_8)_3$. The expected theoretical mass is 4462.4 g/mol, excluding counterions. The maximum observed at m/z = 4463.6 could correspond to the protonated form of the peptide. The peak at 4335.5 could correspond to a missing lysine residue. The subsequent peaks at 4206.4, 4078.7, 3950.2 are also likely lysine deletion products. The small peaks on the extreme left are doubly-charged peaks

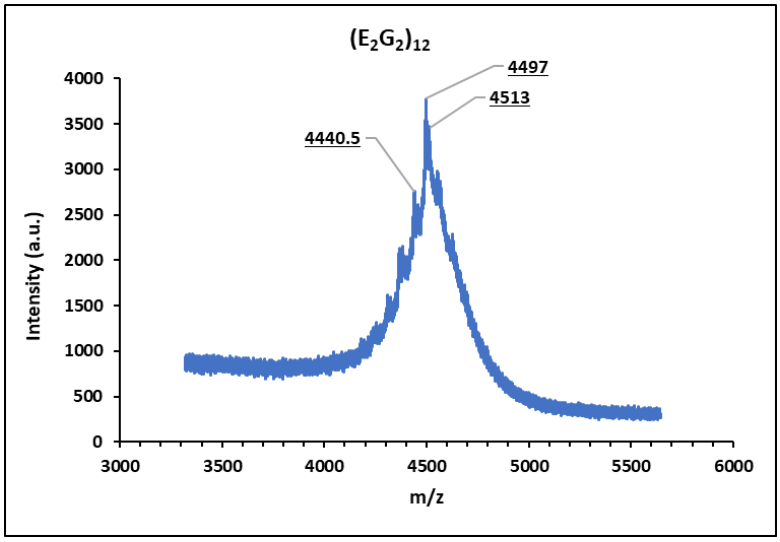

Figure S1g. MALDI spectrum of $(E_2G_2)_{12}$. The expected theoretical mass is 4485 g/mol, excluding counterions. The maximum was observed at m/z = 4497. The peak at 4513 could correspond to the presence of a Na^+ counterion.

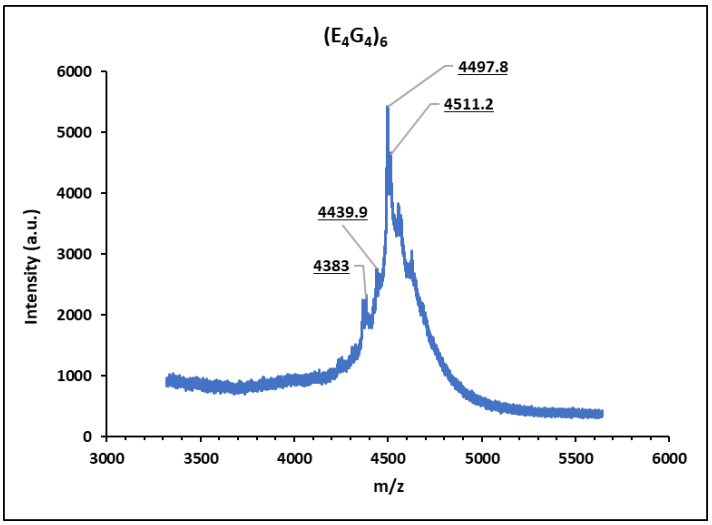

Figure S1h. MALDI spectrum of $(E_4G_4)_6$. The expected theoretical mass is 4485 g/mol, excluding counterions. The maximum was observed at m/z = 4497.8. The peak at 4511.2 could correspond to the presence of a Na^+ counterion.

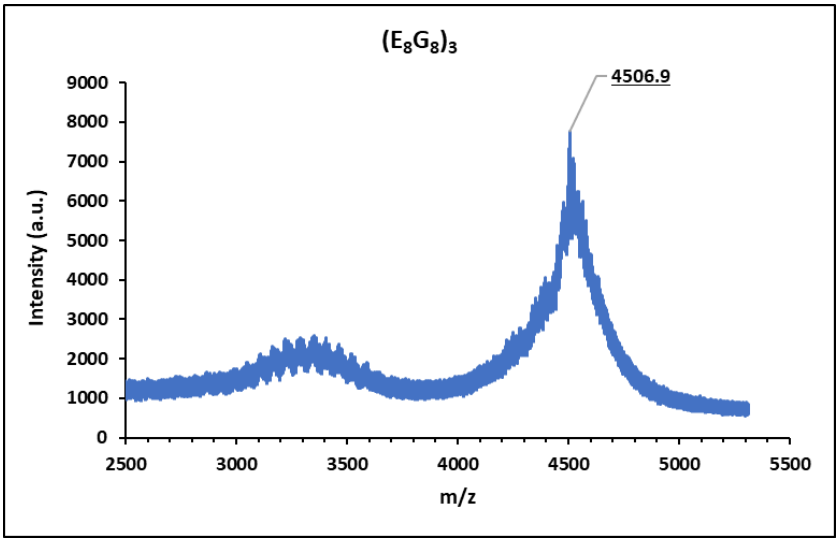

Figure S1i. MALDI spectrum of $(E_8G_8)_3$. The expected theoretical mass is 4485 g/mol, excluding counterions. The maximum was observed at m/z = 4506.9 and could correspond to the presence of a Na^+ counterion.

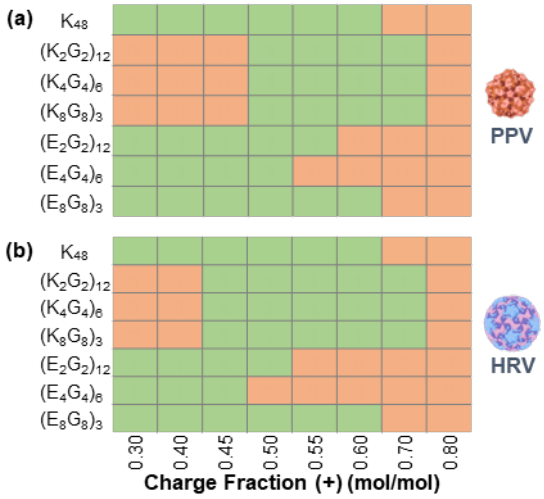

Figure S2. Binary map characterizing turbidity in coacervates. Maps indicating the presence (green) or absence (orange) of turbidity for coacervate samples made from different relative amounts of charge-patterned polypeptides (N = 48) in the presence of **(a)** PPV and **(b)** HRV. For systems where the cationic (K-containing) polypeptide is listed, coacervates were formed with E_{48}. For systems where the anionic polypeptide is listed, coacervates were formed with K_{48}. The turbidity index was noted visually and should be taken as merely a qualitative assessment of the sample.

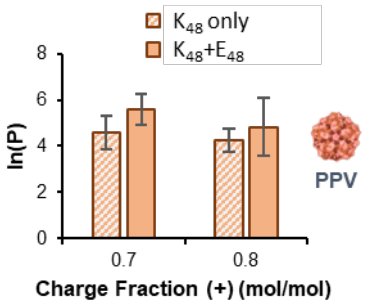

Figure S3. PPV partitioning with and without polyanion. PPV partitioning was measured in simulated dense and supernatant phases created by mixing virus with K_{48} but not E_{48}. The partitioning is compared with the data containing both K_{48} and E_{48} at charge fractions 0.7 and 0.8, which did not form a turbid solution. The data are the average of three experiments with the error bars shown as the standard deviation of the replicate measurements.

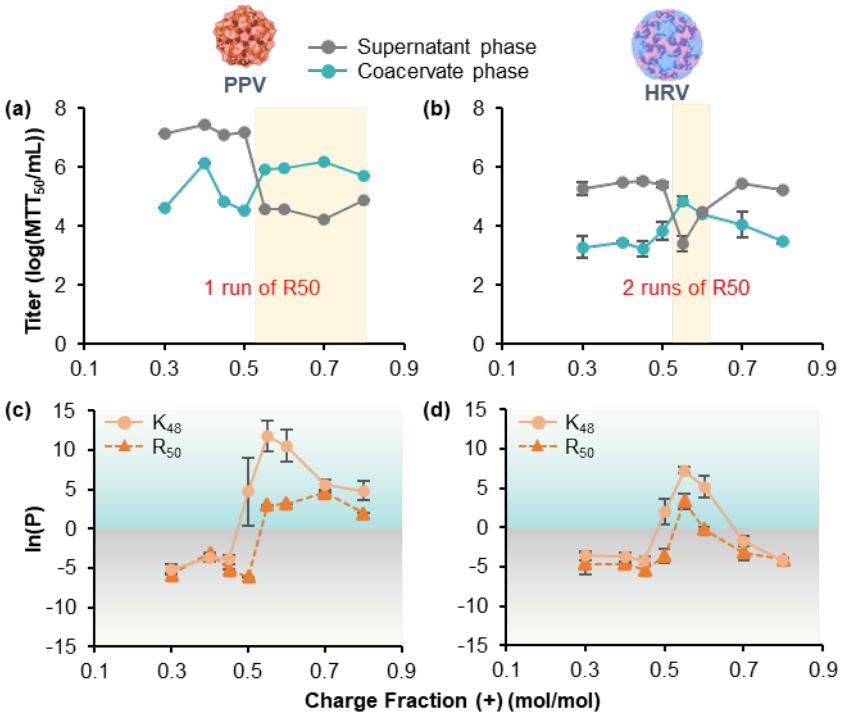

Figure S4. Trends in virus uptake as a function of polycation identity. (a) PPV and **(b)** HRV titers in the supernatant and coacervate phases as a function of charge stoichiometry for coacervates formed from poly(arginine) of chain length N = 50 and poly(glutamate) of chain length N = 48. Yellow boxes highlight the range of charge fractions over which ln(P) > 0. A comparison of the partition coefficient log(P) for **(c)** PPV and **(d)** HRV as a function of charge stoichiometry showing the decrease in partitioning in coacervates composed of R_{50} as compared to K_{48}. The data are the average of three experiments with the error bars shown as the standard deviation of the replicate measurements except where indicated in parts a and b.

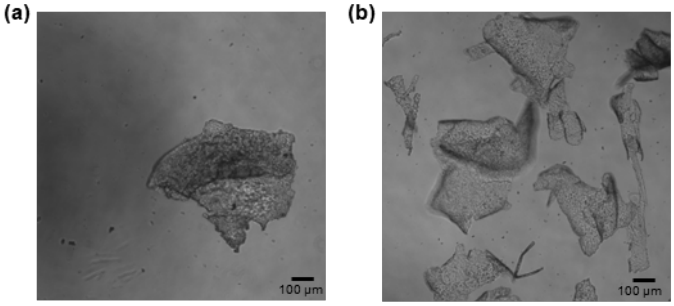

Figure S5. Optical micrographs of precipitate flakes of HRV in arginine-containing complexes. Complexes were prepared from R_{50} and E_{48} at a charge stoichiometry of **(a)** 0.55 and **(b)** 0.60 using an Olympus IX50 microscope at 10X magnification. Similar flakes were observed with PPV (data not shown).

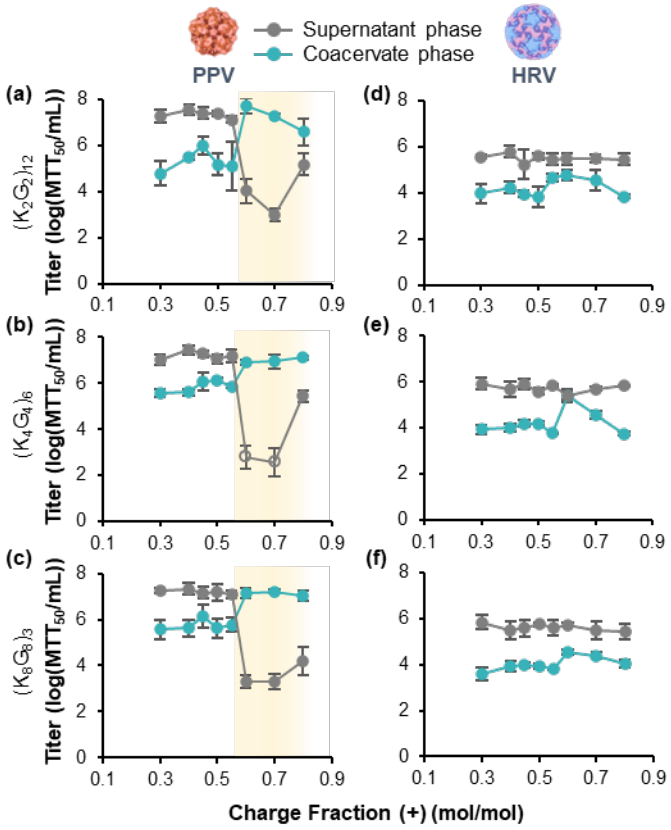

Figure S6. Effect of cationic charge patterning on virus uptake. (a-c) PPV and **(d-f)** HRV titers in the supernatant and coacervate phases as a function of charge stoichiometry for coacervates formed from charge patterned polypeptides (N = 48) of K_nG_n with E_{48}. Yellow boxes highlight the range of charge fractions over which ln(P) > 0. The data are the average of three experiments with the error bars shown as the standard deviation of the replicate measurements. Open symbols indicate the data were measured at the limit of detection.

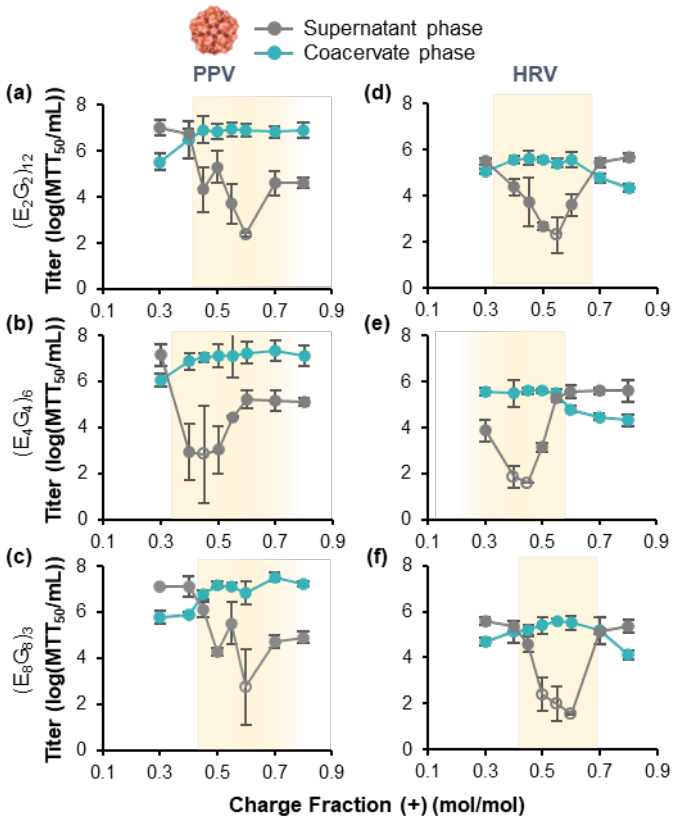

Figure S7. Effect of anionic charge patterning on virus uptake. (a-c) PPV and **(d-f)** HRV titers in the supernatant and coacervate phases as a function of charge stoichiometry for coacervates formed from charge patterned polypeptides (N = 48) of E_nG_n with K_{48}. Yellow boxes highlight the range of charge fractions over which ln(P) > 0. The data are the average of three experiments with the error bars shown as the standard deviation of the replicate measurements. Open symbols indicate the data were measured at the limit of detection.

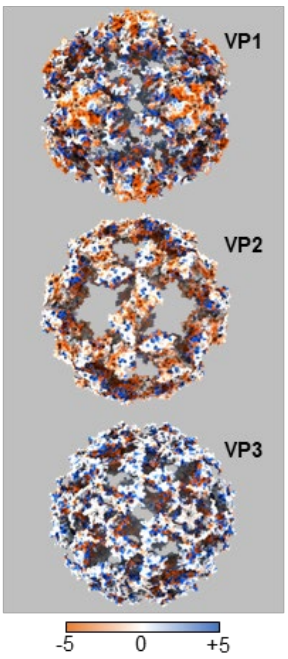

Figure S8. Electrostatic potential distribution on HRV capsomeres. VP1 presents the highest negative potential followed by VP2 and VP3.

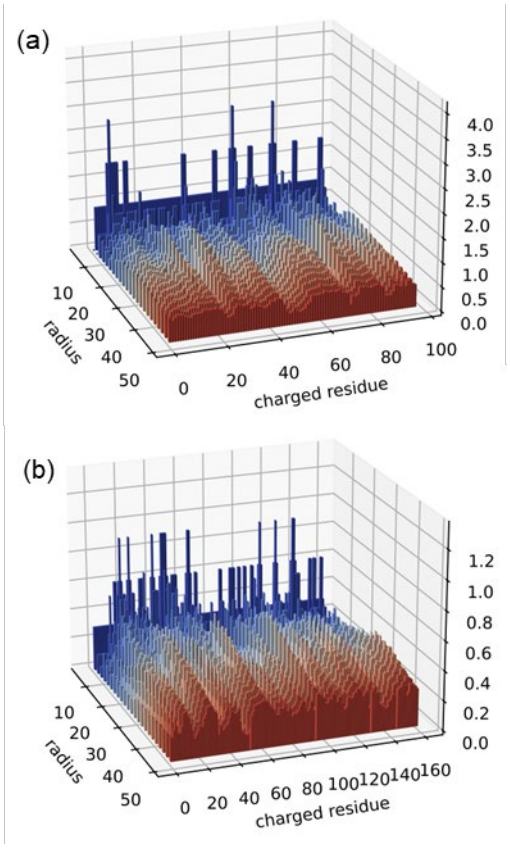

Figure S9. Radial distribution of charge when all residues are taken into account. As compared to Figure 4, here, all charged residues, whether they are on the surface of the virus or not, are taken into account. (a) PPV and (b) HRV.

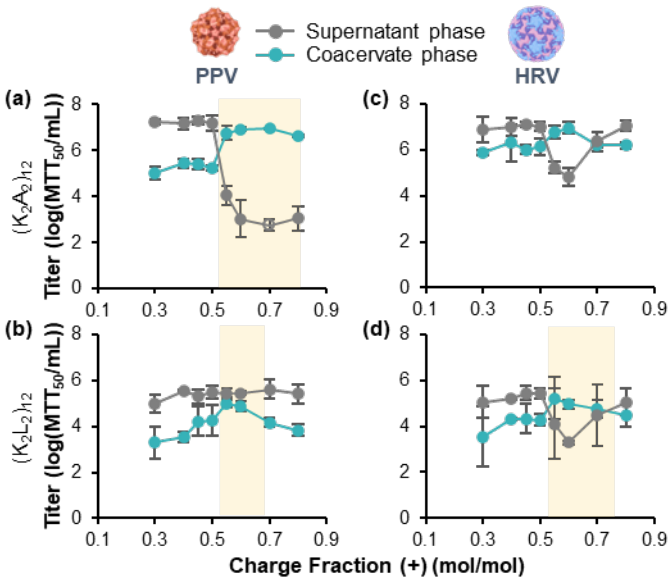

Figure S10. Effect of hydrophobicity on virus uptake. (a,b) PPV and **(c,d)** HRV titers in the supernatant and coacervate phases as a function of charge stoichiometry for coacervates formed from charge patterned polypeptides (N = 48) of **(a,c)** $(K_2A_2)_{12}$ with E_{48} and **(b,d)** $(K_2L_2)_{12}$ with E_{48}. Yellow boxes highlight the range of charge fractions over which ln(P) > 0. The data are the average of three experiments with the error bars shown as the standard deviation of the replicate measurements. Open symbols indicate the data were measured at the limit of detection.

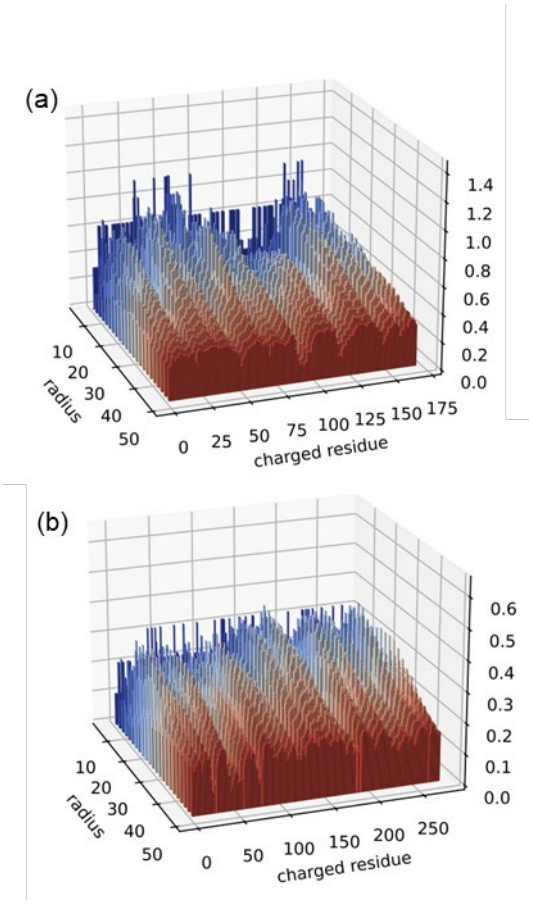

Figure S11. Radial distribution of hydrophobicity when all residues are taken into account. As compared to Figure 6, here, all charged residues, whether they are on the surface of the virus or not, are taken into account. (a) PPV and (b) HRV.